

Article

The Characterization of Coatings Formed on As-Cast Al, Al–Si, and Al–Ca Aluminum Substrates by Plasma Electrolytic Oxidation

Nikolay V. Letyagin ^{1,2,*}, Torgom K. Akopyan ^{1,2}, Alexander A. Sokorev ^{2,3}, Tatiana A. Sviridova ², Stanislav O. Cherkasov ² and Yulbarskhon N. Mansurov ⁴

¹ Sector of Scientific Activity, Moscow Polytechnic University, 38, Bolshaya Semyonovskaya Str., Moscow 107023, Russia; nemiroffandtor@yandex.ru

² Department of Metal Forming, National University of Science and Technology MISIS, 4 Leninsky Pr., Moscow 119049, Russia; sokorev.a@misis.ru (A.A.S.); tim-17@yandex.ru (T.A.S.); ch3rkasov@gmail.com (S.O.C.)

³ JSC Aluminum Alloys Plant, 3K Metallurgov Ave., Podolsk 142155, Russia

⁴ Department of Wagons and Wagon Economy, Tashkent State Transport University, 1, Temiryolchilar Street, Tashkent 100167, Uzbekistan; mansurov_yulbarsxon@tstu.uz

* Correspondence: n.v.letyagin@mospolytech.ru

Abstract: In this study, ceramic coatings were grown on the surface of as-cast aluminum alloys via plasma electrolytic oxidation (PEO). The effect of the Si- and Ca-alloying elements in aluminum on the growth process, morphology, composition, mechanical, and corrosion properties of the PEO coatings was investigated. Uniform coatings with a minimum number of defects were formed on the surfaces of Al–Ca alloys. Increasing the Si content in Al led to an increase in the bulk and surface porosity of the coatings. The α -Al₂O₃ phase mainly formed in the coatings synthesized on pure Al and Al–Ca alloys, while an increased amount of Si in Al alloys hindered the formation of the α -Al₂O₃ phase. The coatings had a microhardness of 660–1180 HV, which was 20–30 times higher than that of the original as-cast alloy. Moreover, the coating on the Al–Ca alloys had the highest peak hardness, which was probably caused by the formation of a greater amount of the α -Al₂O₃ phase. Electrochemical studies in 3.5% NaCl have shown that PEO coatings reduce the corrosion current density. Of all PEO-treated alloys, Al and Al1Ca have the lowest corrosion current density and hence the highest corrosion resistance due to the composition and uniformity of the coating.

Keywords: Al alloys; microstructure; casting alloys; plasma electrolytic oxidation (PEO); coatings; microhardness; XRD analysis; corrosion resistance



Citation: Letyagin, N.V.; Akopyan, T.K.; Sokorev, A.A.; Sviridova, T.A.; Cherkasov, S.O.; Mansurov, Y.N. The Characterization of Coatings Formed on As-Cast Al, Al–Si, and Al–Ca Aluminum Substrates by Plasma Electrolytic Oxidation. *Metals* **2023**, *13*, 1509. <https://doi.org/10.3390/met13091509>

Academic Editor: Rebecca L.

Higginson

Received: 28 June 2023

Revised: 6 August 2023

Accepted: 15 August 2023

Published: 23 August 2023



Copyright: © 2023 by the authors. Licensee MDPI, Basel, Switzerland. This article is an open access article distributed under the terms and conditions of the Creative Commons Attribution (CC BY) license (<https://creativecommons.org/licenses/by/4.0/>).

1. Introduction

The Al–Si alloying system is widely used for the production of the most common aluminum casting alloys. They are characterized by good castability, low hot tearing tendency, and good corrosion properties [1]. However, the development of Al–Ca eutectic-based alloys can significantly improve the performance of conventional aluminum alloys. Due to the relatively large volume fraction of very fine eutectic Al₄Ca phase inclusions, new alloys possess high as-cast strength, thermal stability (due to the high eutectic temperature (614 °C) and extremely low solubility of Ca in aluminum), and processability at deformation, with high reduction rates [2,3]. Alloys containing various amounts of calcium and alloying elements such as Fe, Si [4], Mn [5], Cu [6], REM (Ce, La) [3,7], Ni [8], Zn, Mg [9], Sc, and Zr [10] have been studied with regard to these structural, technological (casting [7,11,12], deformation treatment [10], and additive manufacturing [13]), and mechanical properties. This has helped to clarify the influence of the structure and phase composition on the mechanical and technological properties of aluminum–calcium alloys. Another promising

area of research is the study of the capability of the coatings to increase the lifetime of industrial Al–Ca alloys.

Plasma electrolytic oxidation (PEO) is an advanced surface treatment technology for the formation of protective ceramic coatings on lightweight materials (Al, Mg, and Ti, etc.) that has excellent properties, such as high hardness and good wear/corrosion resistance [14–16]. Moreover, the PEO process is environmentally friendly due to the use of alkaline-water-based electrolytes and ensures high output, enabling the production of ceramic coatings quickly, e.g., in 30–40 min [15,17,18]. Some good examples of PEO application are the mass production of PEO-coated aluminum items for the oil and gas industry [19], and moving mechanisms for marine and aircraft engineering and the automotive industry [20,21].

At the same time, the composition of the substrate used has a significant effect on the properties of PEO coatings. In this work, a systematic study on the individual effects of Si [22–24], Cu [25,26], Mg [27], Sn [28], Zn [29], Ce [30], Mn [31], and Ni [32] on the PEO behavior of binary Al alloys in silicate–alkaline electrolytes is reported. We show that the main structural components of PEO coatings on aluminum alloys are α -Al₂O₃, γ -Al₂O₃, and silicon oxide (mullite). The ratio of these oxides is determined by the elemental composition of the substrate. Increasing the number of alloying elements in the binary aluminum alloys hinders α -Al₂O₃ formation in PEO coatings, which in turn leads to a decrease in the hardness and tribological characteristics of the coatings. Furthermore, the porosity and number of cracks in the coatings tend to grow with an increase in the content of alloying element ions in the coating.

A detailed study of PEO coatings on conventional Al–Si alloys showed that the properties of the coatings largely depend on the particle size of the silicon eutectic phase [23,33–37]. The presence of Si particles produces local current shielding during the PEO process since Si oxidation requires a higher voltage than Al oxidation. This effect leads to the formation of an uneven coating in the eutectic region. The latter issue can be solved by reducing the size of the eutectic particles. For example, strontium-modified eutectic silicon particles with lengths of 5–8 microns and widths of about 0.5–1 microns contribute to the formation of more homogeneous and dense coatings with higher corrosion resistance [23]. Meanwhile, the results of studies of PEO coatings on aluminum alloys obtained using additive technologies (AT) also demonstrate the above-described trend. A distinctive feature of the materials obtained with AT is the ultra-fine structure of the eutectic formed at elevated cooling rates during selective laser melting [33]. The thickness and porosity of the coatings increase with the Si content in the substrate. Coatings formed on Al–Si alloys with a silicon content of up to 2 wt.% consist mainly of α -Al₂O₃, while further increases in the Si content led to significant changes in the α -Al₂O₃/ γ -Al₂O₃ ratio, with the γ -Al₂O₃ fraction becoming predominant [18]. This change in the phase composition leads to a decrease in the average microhardness of the coatings.

However, to the best of our knowledge, there have been no studies dealing with the specific features of the growth of PEO coatings on Al–Ca-based alloys. In this work, a comprehensive study of the structure, phase composition, and mechanical properties of PEO coatings built up on a base binary Al1Ca alloy was carried out, and a comparison was made with coatings on a binary Al4Si alloy and pure aluminum. The model Al1Ca alloy was chosen due to the fact that the calcium concentration in this alloy is universal, i.e., it can act as a small additive for improving the manufacturability and properties of Al–Zn–Mg-system alloys [9] or as the base composition for the development of new aluminum–calcium alloys [7,12]. The Al4Si alloy composition was chosen because its eutectic phase makes up almost the same proportion as that of the Al1Ca alloy. It is also of particular interest to compare the effect of alloying elements (Si and Ca) and PEO coatings on the corrosion behavior of aluminum alloys.

2. Materials and Methods

Three model alloys, i.e., Al (purity 99.9%), Al₄Si, and Al₁Ca, were selected for a comparison of coatings formed by plasma electrolytic oxidation. The alloys were prepared from high purity aluminum (99.99%) in a resistance furnace with a graphite crucible. The selected compositions were prepared from an Al-10% Ca binary master alloy and pure Si. After the melting of the basic components, the melt was held for 5–10 min for homogenization and slag removal, and the metal was then cast into a graphite mold with a working cavity of 10 × 40 × 180 mm at 780–800 °C.

The coatings were formed using a PEO installation with a 250 kW high-frequency high-voltage switching power supply unit. The PEO process was conducted in a silicate-alkaline electrolyte containing 2 g/L KOH, 6 g/L Na₂SiO₃, and 1 g/L H₃BO₃ in distilled water. The electrolyte was homogenized by stirring, and its temperature near the electrolyte cell was kept at 15–20 °C during PEO coating deposition. The following electrical parameters were maintained during coating formation: anode voltage $U_a = 1000$ V; cathode voltage $U_k = 300$ V; current density 25 A/dm²; and pulse frequency $f = 3$ kHz. The PEO process durations were 10, 20, 30, and 40 min.

The thickness of the PEO coatings was measured at 20 randomly selected points using Elcometer 456, and the average values were calculated.

The microstructure of the castings was examined by means of optical microscopy (OM). The morphology and elemental compositions of the surfaces and cross-sections of the PEO coatings were examined using scanning electron microscopy (SEM, TESCAN VEGA 3, Brno, Czech Republic) and electron microprobe analysis (EMPA, OXFORD AZtec). X-ray diffraction (XRD) data were obtained at room temperature using a DRON-4 diffractometer in Co K α radiation and analyzed with a software package [38]. XRD profiles were taken in a 2 θ range of 10 to 130 deg with a 0.1 deg step and a 3 s exposure.

The sizes of pores in the external PEO layers were estimated using an Alpha-Step 200 stylus-based surface profiler (Tencor Instruments, Milpitas, CA, USA).

Microhardness measurements were conducted using DUROLINE MH-6 (Metkon, Bursa, Turkey). The Vickers indentation loads were 50 g, and the dwell time was 5 s.

Electrochemical characterization included polarization curve measurements with an IPC-Pro electronic potentiostat. The test medium was a 3.5% NaCl solution. The samples were polarized from the cathodic region to the anodic one at a potential sweep rate of 1 mV/s. The reference electrode was saturated Ag/AgCl₂, and the auxiliary electrode was platinum. The polarization experiments were conducted three times for different samples and showed them to be similar.

3. Results

The as-cast Al, Al₄Si, and Al₁Ca alloys were treated using PEO technology. The hypoeutectic Al₄Si and Al₁Ca alloys (Figure 1) consisted of α -Al dendritic cells surrounded by eutectic structures ((Al) + (Si)) and ((Al) + Al₄Ca), respectively). However, the dendritic cells of the Al–Ca alloy had smaller sizes. The actual chemical compositions of the alloys summarized in Table 1 were quite close to the nominal one. The microstructures of those alloys contained similar volume fractions of the eutectic phases formed during solidification, i.e., about 3 vol.%. Moreover, it is worth mentioning that a comparable volume fraction of the second phase in the Al–Ca alloy was achieved at a significantly lower concentration of the main alloying component.

As noted above, surface treatment of the Al–Si alloys remains a difficult task since silicon-rich phases can hinder the homogeneous growth of oxide layers. Thus, it is of particular interest to compare the PEO process for alloys of the Al–Ca and Al–Si systems and to clarify the basic mechanisms of the influence of Ca as a new alloying element on the PEO process.

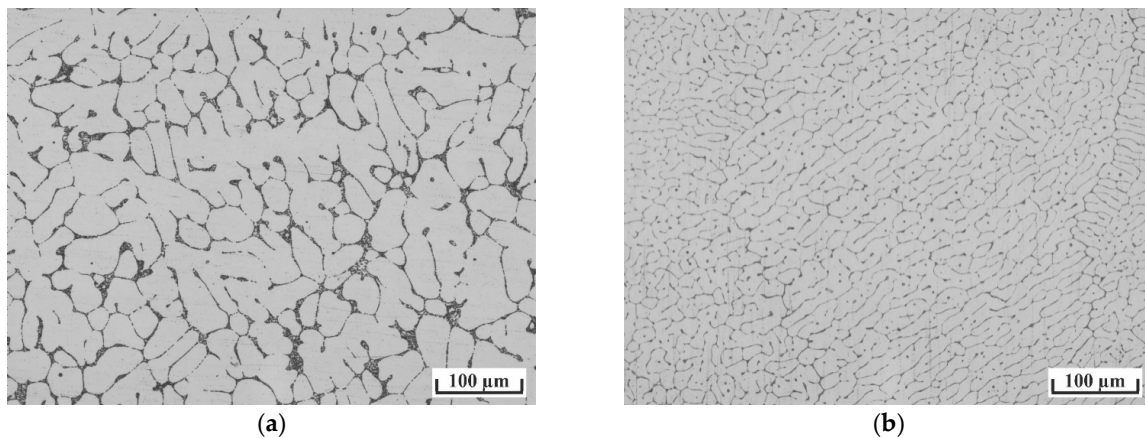


Figure 1. Microstructure of (a) Al4Si and (b) Al1Ca as-cast alloys.

Table 1. Actual chemical composition (wt.%), calculated eutectic fraction (Q, wt.%, (vol.%)), and Vickers hardness (HV) of the alloys.

No.	Alloy	Actual Chemical Composition, wt.%			Q, wt. % (Vol. %)	HV
		Al	Si	Ca		
1	Al	99.99	-	-	-	17
2	Al4Si	95.80	4.20	-	2.70 (3.10)	43
3	Al1Ca	99.10	-	0.80	2.95 (3.44)	27

3.1. Kinetics of PEO Coatings Formation

Figure 2 shows the thicknesses of coatings on pure aluminum and the eutectic Al–Si and Al–Ca alloys for different PEO treatment durations. Both the Al and Al–Ca samples exhibited similar coating growth rates within the first 30 min, and then the growth rates decreased. Similar behavior was observed for the Al–Si system alloy. However, a characteristic feature of the Al–Si alloy is a low PEO coating growth rate in the first 10 min of the process. The coatings grew to almost similar thicknesses of about 39–42 μm after 30 min PEO treatment for all the samples.

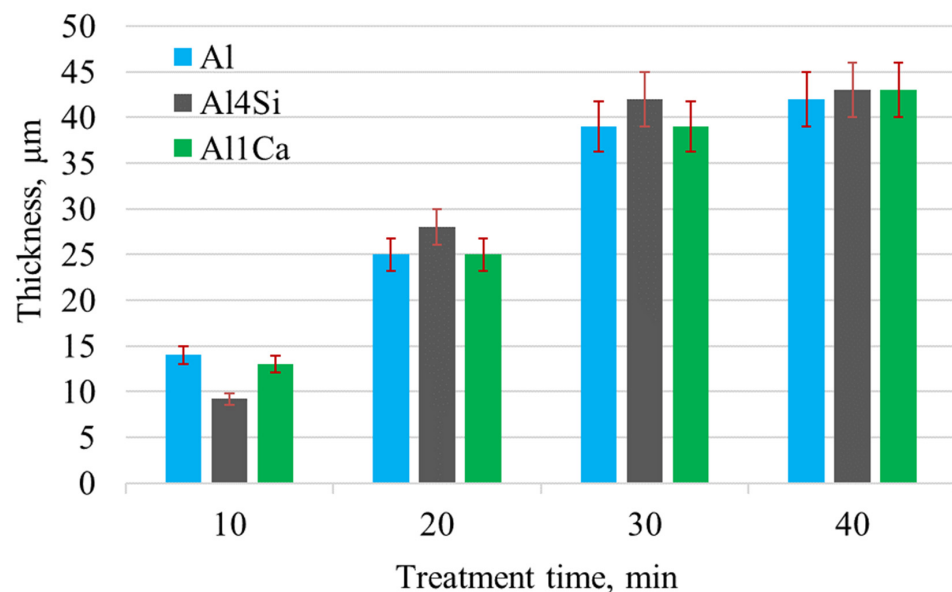


Figure 2. Kinetics of PEO coating formation as a function of time for the PEO treatment of Al, Al4Si, and Al1Ca aluminum substrates.

For a better understanding of the processes accompanying PEO treatment, the surface and cross-sectional microstructures of the coatings obtained after 30 min PEO treatment (Figure 3) were studied.

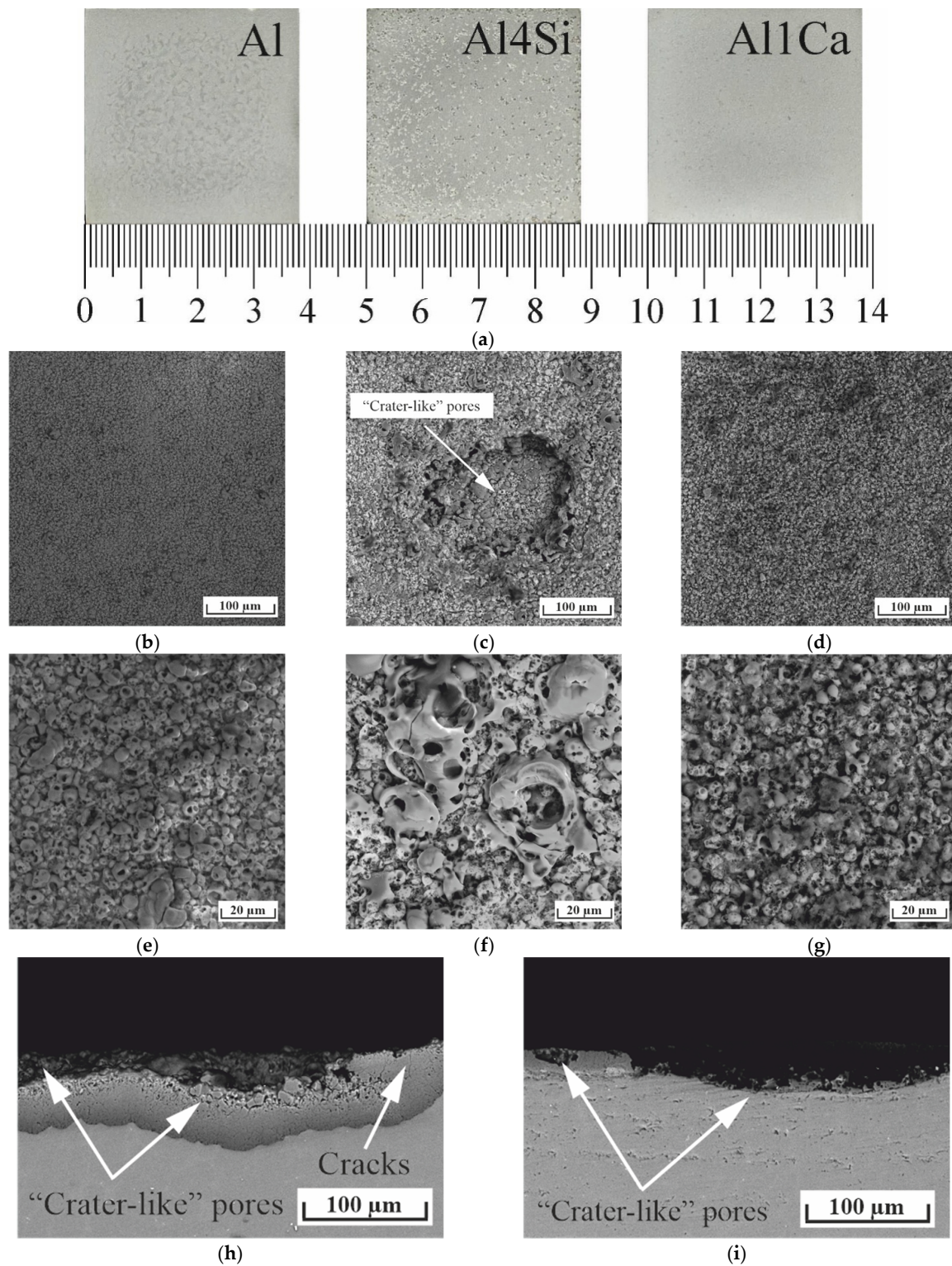


Figure 3. (a) Appearance of aluminum substrates with PEO coatings synthesized in the base electrolyte during 30 min; micrographs of the loose outer layer of the PEO coating (SEM): (b,e) Al, (c,f) Al4Si, (d,g) Al1Ca; and typical defects of the PEO coatings synthesized on the Al4Si alloy (cross-section view) (h,i).

3.2. Surface and Cross-Sectional Microstructure of PEO Coatings

The appearance of the coatings on the aluminum substrates after 30 min of PEO treatment is shown in Figure 3a. Figure 3b–g shows typical top-view micrographs of the outer coating layer. The coatings grown on pure aluminum and the Al1Ca alloy had the highest uniformity. As for the Al–Si system alloy, the morphology of the as-grown coating appeared to be coarser. Figure 3c shows that the “crater-like” pores in the coating formed on the Al–Si alloy can be as large as 200 microns. Stylus-based surface profiling of pores in the external PEO layers of the Al–Si alloy showed that the average depth of the pores was 23 to 33 μm , with their diameter being about 200 μm . Typical defects (cracks and “crater-like” pores) of the PEO coatings synthesized on the Al4Si alloy (cross-section view) are shown in Figure 3h,i.

Thus, uniform coatings with small numbers of defects were formed on the surface of pure aluminum and the Al–Ca alloy. Increasing the amount of Si in Al led to the formation of multiple pores on the coating surface.

According to the EDS results (Figure 4), the coatings synthesized in the silicate-alkaline electrolyte were saturated with silicon atoms which were distributed over the whole coating surface. Moreover, the formation of Ca-rich regions in the outer layers was observed for the Al–Ca alloy. One can assume that they were caused by a specific Si distribution.

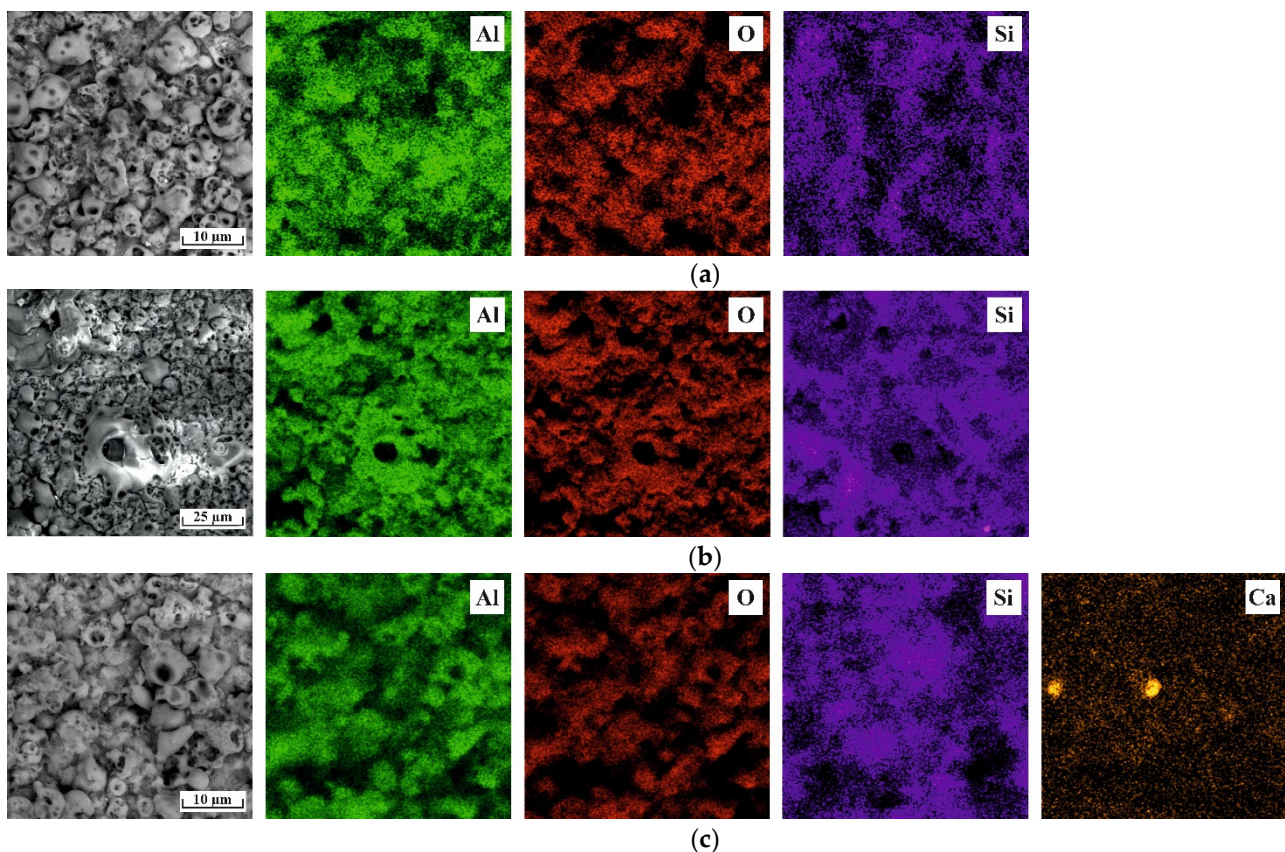


Figure 4. EDS distribution maps for the surfaces of the PEO coatings: (a) Al, (b) Al4Si, and (c) Al1Ca.

According to the element distribution map (Figure 5), Si was preferentially located in the top parts of the coatings. Probably, it was in the form of silicon dioxide formed as a result of the thermochemical treatment, during which the electrolyte surrounded the working electrode. According to the experimental results, the Si-containing region in the Al4Si specimen was significantly thicker than those for the Al and Al1Ca PEO coatings, due to the incorporation of Si-rich electrolyte species. A specific feature of the coating formed on the Al–Ca sample was the presence of a thin calcium-containing region in its top part.

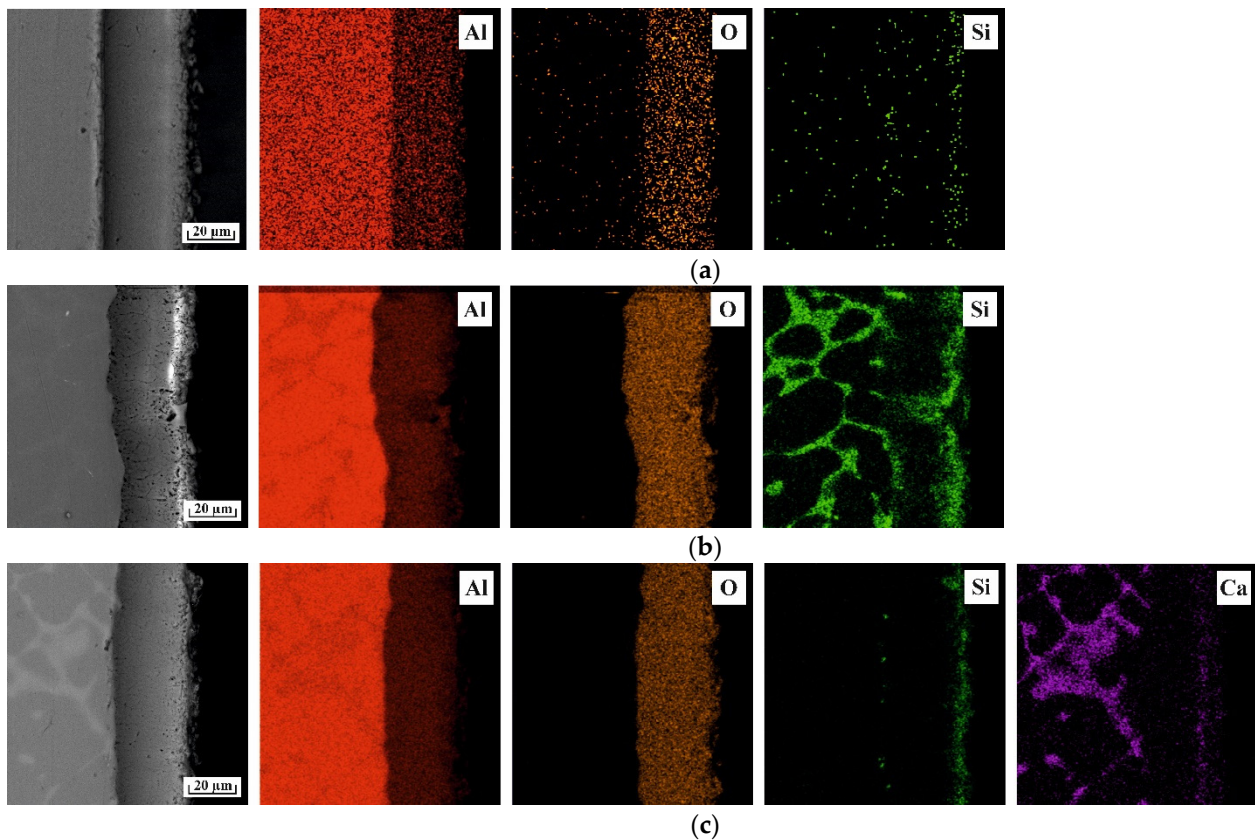


Figure 5. Cross-sectional element distribution maps for PEO coatings formed on various aluminum substrates: (a) Al, (b) Al₄Si, and (c) Al₁Ca.

Figure 6 shows the distributions of the main elements between the substrate and the PEO coating over the entire thickness of the layers. One can see that the distributions of aluminum migrating from the substrate and oxygen were relatively stable in the bulk of the PEO layers. However, the aluminum content decreased and the silicon content increased significantly near the coating surface. A significant growth in the calcium peak for the coating on aluminum-calcium alloys can be observed for the Al–Ca alloy.

SEM cross-sectional data for the PEO coatings show that the inner structures of the coatings formed on pure aluminum and Al₁Ca are distinguished by a relative density and the smallest number of defects (Figure 6). The coating formed on the Al₄Si alloy had a well-developed pore system in the inner layer. Such an inhomogeneous structure can be associated with a layer-by-layer change in the chemical composition in the depth of the PEO coating.

It is worth mentioning that the surfaces of the coatings formed on pure aluminum and the Al–Ca alloy were quite uniform. For example, in the presence of the Al–Si eutectic phase the interfaces between the oxide layer and the base metal became wave-like.

3.3. X-ray Diffraction Analysis

Based on the XRD data (Figure 7, Table 2), the PEO coatings on Al and the Al–Ca alloy mainly consisted of high-temperature α -Al₂O₃ modification and γ -Al₂O₃. The volume fractions of α -Al₂O₃ and γ -Al₂O₃ were about 60 and 30%, respectively. However, the elements migrating from the substrate had a great influence on the α -Al₂O₃/ γ -Al₂O₃ ratio. For example, the coating formed on the Al₄Si alloy consisted almost entirely of γ -Al₂O₃.

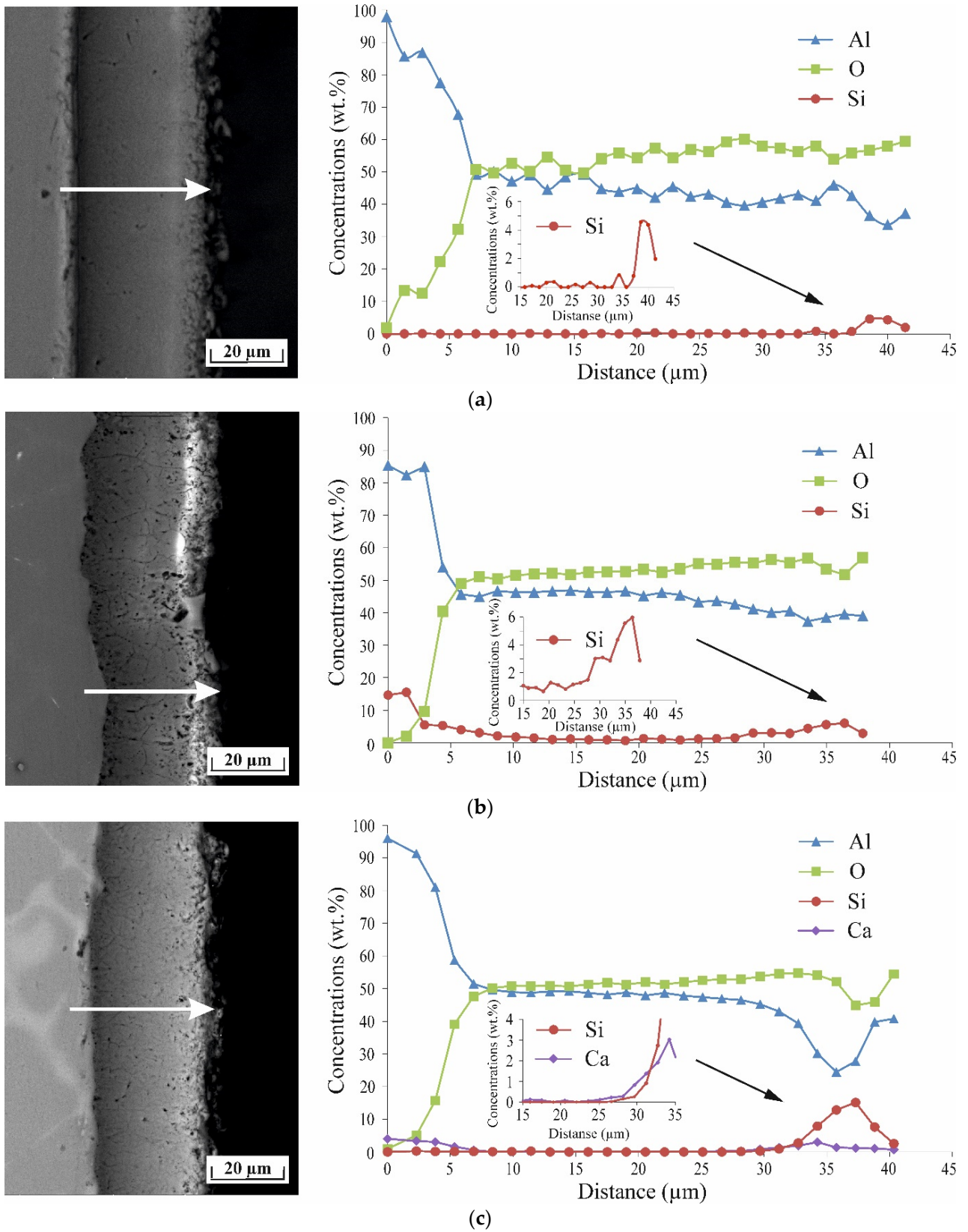


Figure 6. Distribution of main elements in PEO coatings formed on various aluminum substrates: (a) Al, (b) Al₄Si, and (c) Al₁Ca.

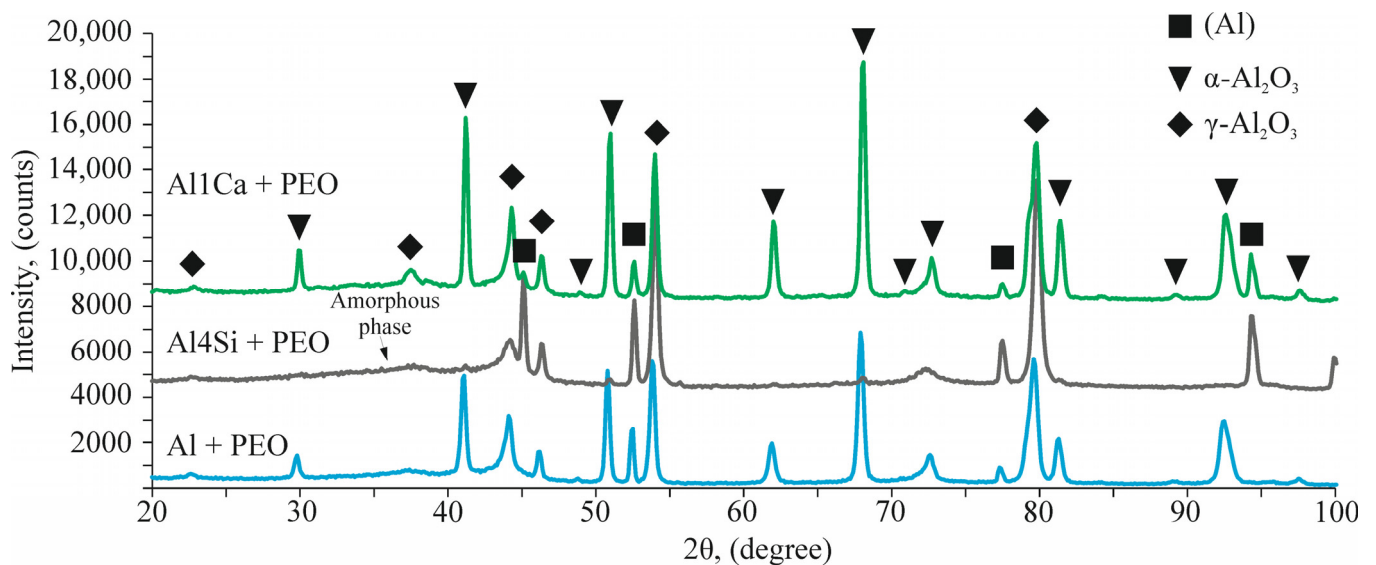


Figure 7. XRD patterns of PEO coatings grown on various aluminum substrates.

Table 2. XRD data of PEO coatings grown on various aluminum substrates.

No	Alloy, wt.%	Phase	Pearson Symbol	Volume Fraction, %	Lattice Parameters, Å	
					a	c
1	Al (purity 99.9%)	Al	cF4/1	2.7 ± 0.1	4.049	-
		α-Al ₂ O ₃	hR10/1	60.1 ± 0.3	4.758	12.997
		γ-Al ₂ O ₃	cF120/4	37.1 ± 0.3	7.903	-
2	Al4Si	Al	cF4/1	21.1 ± 0.2	4.047	-
		α-Al ₂ O ₃	hR10/1	1.4 ± 0.1	-	-
		γ-Al ₂ O ₃	cF120/4	77.5 ± 0.2	7.896	-
3	Al1Ca	Al	cF4/1	7.6 ± 0.1	4.050	-
		α-Al ₂ O ₃	hR10/1	62.3 ± 0.3	4.759	12.994
		γ-Al ₂ O ₃	cF120/4	30.1 ± 0.3	7.904	-

3.4. Microhardness of PEO Coatings

Microhardness measurements were carried out for polished coating cross-section samples. The central parts of the coatings were analyzed (Figure 8). The average microhardness values of the coatings formed on the pure aluminum and Al–Ca alloy substrates were 955 (740–1180 HV range) and 991 (840–1150 HV), respectively (Table 3). The coatings formed on the silicon-containing substrates exhibited a decrease in the average hardness to 843 HV. The microhardness distribution histograms based on twenty measurements suggest that the Al–Si cast alloy contained a greater number of softer regions with a hardness of 660–1030 HV. However, despite the significant influence of the substrates on the hardness of the coatings, their formation on the surfaces of aluminum alloys can significantly increase the microhardness of the alloy surfaces. The initial microhardness values of the Al, Al1Ca, and Al4Si alloys were about 17, 27, and 43 HV, respectively.

Table 3. Average microhardness (min–max) in the middle of the coatings.

Alloy	Microhardness, HV
Al (purity 99.9%)	955 (740–1180)
Al4Si	843 (660–1030)
Al1Ca	991 (840–1150)

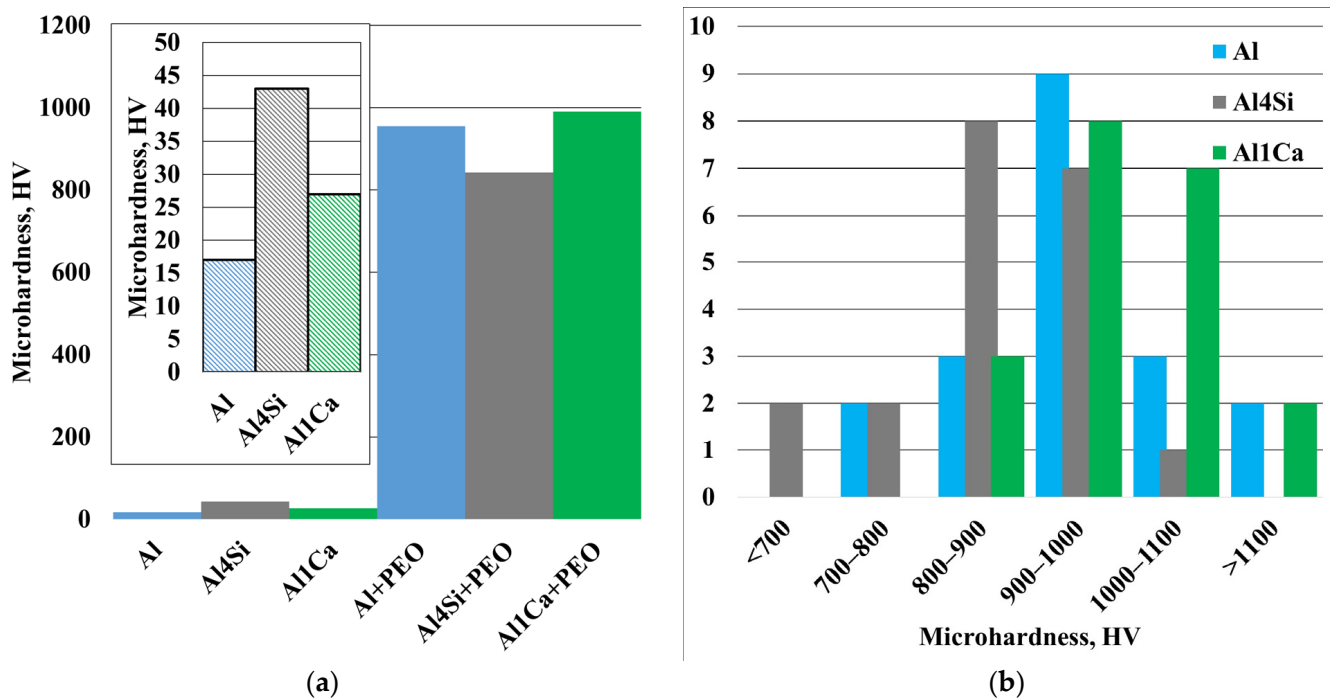


Figure 8. (a) Average microhardness of alloys and PEO coating; (b) hardness distribution histogram at half-thickness of PEO coating.

3.5. Electrochemical Behavior of PEO Coatings

Figure 9 shows the polarization diagrams of the test Al alloys. For a quantitative analysis and comparison of the effect of alloying elements (Si and Ca) on the corrosion resistance of the PEO coatings, the corrosion current densities (I_{corr}) were determined using polarization curve extrapolation and corrosion potential (E_{corr}) measurements [39]. In all cases, the cathodic branches had significant slopes (bottom curves), suggesting a cathodic-controlled corrosion reaction [40]. Table 4 summarizes I_{corr} and E_{corr} for the test samples. It can be seen that the addition of 4% Si to pure Al led to an increase in the corrosion current density (I_{corr}) compared to that of pure Al (18.3×10^{-3} and 8.2×10^{-3} mA/cm², respectively). Ca addition to pure Al caused the formation of micro-galvanic pairs between Al and Al₄Ca, which in turn led to the facilitation of both the cathodic and anodic processes, with a corresponding increase in the corrosion current density of the Al1Ca alloy in comparison with that of pure Al (pure Al: 8.2×10^{-3} , Al1Ca: 10.1×10^{-3} mA/cm²).

Table 4. Results of potentiodynamic corrosion tests in 3.5% NaCl solution for uncoated alloys and PEO-coated alloys.

Sample	Corrosion Potential, E_{corr} (mV)	Corrosion Current Density, i_{corr} (mA/cm ²)
Al (purity 99.9%)	−625	8.2×10^{-3}
Al (purity 99.9%) + PEO	−506	1.56×10^{-3}
Al4Si	−570	18.3×10^{-3}
Al4Si + PEO	−258	4.2×10^{-3}
Al1Ca	−745	10.1×10^{-3}
Al1Ca + PEO	−203	1.9×10^{-3}

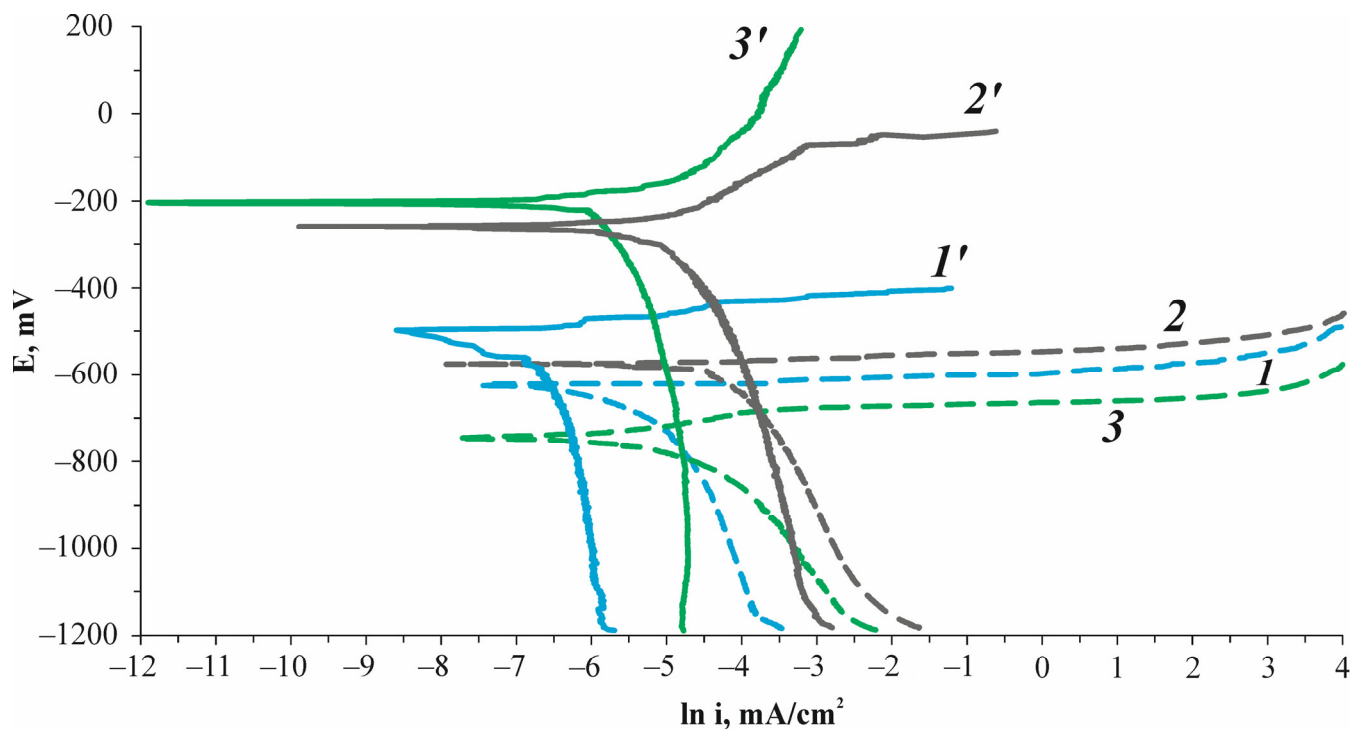


Figure 9. Polarization dependences of the current density, $\ln i$, on the potential E in 3.5% NaCl solution at a potential sweep rate of 1 mV/s for pure alloys (1) Al, (2) Al4Si, and (3) Al1Ca and for PEO-coated alloys (1') Al, (2') Al4Si, and (3') Al1Ca. Potentials are shown relative to silver chloride electrode (Ag/AgCl).

The polarization curves (Figure 9) show that the PEO coatings shifted the steady-state electrode potential to the positive potential area in all cases. The currents of all the cathodic and anodic polarization curves for the PEO-coated samples (Table 4) were lower than those for the uncoated aluminum alloy, suggesting that the coatings have protective properties. Of all the test PEO-treated alloys, the Al4Si alloy had the highest corrosion current density (4.2×10^{-3} mA/cm²) and therefore the lowest corrosion resistance, followed by Al1Ca (1.9×10^{-3} mA/cm²) and Al, which had the lowest corrosion current density (1.56×10^{-3} mA/cm²).

4. Discussion

The test Al4Si and Al1Ca eutectic alloys with equal extra phase volume fractions proved to have fundamental differences in the formation and final properties of the obtained coatings. It should be noted that the surfaces of the coatings forming on pure aluminum and the Al–Ca alloy were quite uniform. However, a different situation was observed for the Al–Si alloy. The growth of the oxide layer seemed to be more controlled by the microstructure of the substrate. For example, in the presence of the Si eutectic phase, the interface between the oxide layer and the base metal became wave-like [22]. This was probably caused by coating growth around the eutectic phase, leading to local thinning of the coating. This is in agreement with the coating growth kinetic curves, which suggest a decrease in the growth rate of the coatings in the first minutes of the process. The highly uniform coatings formed in the inner and outer layers of pure aluminum and the Al1Ca alloy contained the smallest numbers of defects. However, it was the contrary for the coatings grown on the Al–Si alloy. The outer layers of the Al4Si samples contained numerous “crater-like” pores with diameters of 100–200 μm and an average depth of 23 to 33 μm , significantly violating the uniformity of the coatings. An increase in the Si content led to the formation of a well-developed pore system in the inner layer. The parameters of

the coatings formed on the Al–Si alloys and possible mechanisms of defect formation in the coatings have been analyzed in detail [22].

A detailed analysis of the XRD and cross-sectional SEM and SEM–EDS results revealed that the presence of Si and Ca in the substrates influences both the coating formation processes and the content of those elements in the coatings. It should be noted that, the second phase volume fraction being comparable, the effect of silicon on the phase composition of the coatings is significant. Earlier studies [22] showed that Si can suppress the formation of α -Al₂O₃, which is confirmed by the results reported in this work. The coating formed on the Al4Si alloy consisted almost completely of γ -Al₂O₃, whereas the coatings formed on pure aluminum and the Al1Ca alloy had almost equal α -Al₂O₃/ γ -Al₂O₃ ratios. The volume fraction of α -Al₂O₃ was the highest; the volume fractions of α -Al₂O₃ and γ -Al₂O₃ were about 60 and 30%, respectively. Along with the oxidation of Al, Si could also oxidize to form SiO₂ in the high-temperature environment of molten Al during the PEO process [34]. However, no SiO₂ peak was found in the XRD pattern. Probably, the low concentration of Si-containing oxide or its low crystallinity does not allow it to be detected by XRD. Obviously, diffuse scattering in the 25 to 40 deg range shown in Figure 7 indicates the presence of an amorphous phase, most likely SiO₂. The same situation is observed for calcium.

The revealed changes in the phase composition of the coatings had a significant effect on their mechanical properties. However, the average microhardness values of the coatings formed on Al and Al1Ca were almost the same (955 and 991, respectively). The higher γ -Al₂O₃ volume fraction in the Al4Si alloy coating contributed to the reduction in its microhardness to 843 HV.

For all the test alloys, silicon and calcium additions to pure aluminum reduced their corrosion resistance. The addition of 4% Si to pure Al led to an increase in the corrosion current density (I_{corr}) in comparison with that for pure Al (18.3×10^{-3} and 8.2×10^{-3} mA/cm², respectively). This behavior originates from the fact that Si acts as a cathodic structural component in the Al–Si alloys and formed numerous micro-galvanic couples with Al. Indeed, Si facilitates the cathodic process (by lowering its overvoltage), which in turn accelerates the anodic dissolution of Al and the related decrease in the corrosion resistance of the alloy [41,42]. It should be noted that the cathodic structural components shifted the corrosion potential (E_{corr}) towards positive values from -625 mV for pure Al to -570 mV for Al4Si due to the more positive standard potential of Si. One should also bear in mind that the corrosion resistance of the Al1Ca alloy was significantly higher than that of the Al4Si alloy. It was reported [2,43] that the Al1Ca alloy contains the Al + Al₄Ca eutectic phase. Due to the very low standard potential of Ca (approx. -2.76 V), the Al₄Ca phase inclusions acted as anodic regions, which shifted the corrosion potential towards negative values (pure Al: 625 mV, Al1Ca: 745 mV). Ca addition to pure Al led to the formation of micro-galvanic pairs between Al and Al₄Ca, which in turn facilitated the cathodic and anodic processes, and hence increased the corrosion current density of the Al1Ca alloy in comparison with that for pure Al (pure Al: 8.2×10^{-3} mA/cm², Al1Ca: 10.1×10^{-3} mA/cm²). However, one should take into account that the corrosion resistance of the Al1Ca alloy was significantly higher than that of the conventional Al4Si casting alloys.

It was observed for all the samples that PEO treatment effectively increased the corrosion resistance, mainly showing itself in a decrease in the corrosion current density and an increase in the corrosion potential. This behavior originated from the barrier effect of the coating layer, which prevented the interaction between the electrolyte and the alloy [38]. Of all the test PEO-treated alloys, the Al4Si alloy had the highest corrosion current density (4.2×10^{-3} mA/cm²) and hence the lowest corrosion resistance, followed by Al1Ca (1.9×10^{-3} mA/cm²) and Al, with the lowest corrosion current density (1.56×10^{-3} mA/cm²). The main cause of this behavior was the fact that the PEO coating on the Al4Si alloy contained more pores. According to earlier data [44,45], the volume fraction of pores could influence the corrosion properties of alloys. Indeed, the subsequent

decrease in the porosity of Al1Ca and Al led to a decrease in the current densities of these materials to 1.9×10^{-3} and 1.56×10^{-3} , respectively. However, the phase composition and the presence of Ca in the coatings (Figures 5 and 6) could further increase the corrosion resistance [21] of the coatings formed on Al and the Al–Ca alloys.

5. Conclusions

The surfaces of Al and the Al4Si and Al1Ca eutectic alloys were treated with PEO. The coating formation process was studied using growth kinetics monitoring and the characterization of the final coatings (appearance, phase analysis, elemental distribution, microhardness, and electrochemical behavior). The results were as follows.

- (1) The manufacturability of the Al–Ca alloy in terms of the formation of oxide coatings on their surface was confirmed. The presence of Al₄Ca eutectic colonies did not affect the kinetics of coating growth in comparison with pure aluminum.
- (2) Despite the comparable volume fractions of the eutectic phases in the Al4Si and Al1Ca alloys, there were noticeable differences in the porosity, phase composition, and mechanical properties of the coatings. Increasing the amount of Si in Al led to higher internal and surface porosity of the coatings. Uniform coatings with the smallest number of defects were formed on the surface of pure aluminum and the Al–Ca alloy. The phase composition and mechanical properties of the coating on the Al–Ca alloy were close to those for pure aluminum.
- (3) The α -Al₂O₃ phase was predominant in the coatings on pure Al and the Al–Ca alloy, while Si addition to pure Al hindered the formation of the α -Al₂O₃ phase.
- (4) The microhardness of the coatings varied in the 660–1180 HV range, which was 20–30 times higher than that for the uncoated base alloys. The coating on the Al–Ca alloy exhibited the highest peak hardness due to the formation of a greater fraction of the α -Al₂O₃ phase.
- (5) Electrochemical studies showed that silicon and calcium additions to pure aluminum led to an increase in the corrosion activity, but Al1Ca exhibited a greater corrosion resistance than the conventional Al4Si casting alloys. It was found that PEO coatings significantly increased the corrosion resistance of all the studied alloys, mainly showing itself in a decrease in the corrosion current density and an increase in the corrosion potential. Of all the PEO-treated alloys studied, Al and Al1Ca had the lowest corrosion current density and hence the highest corrosion resistance due to the composition and uniformity of the coating.

Author Contributions: Conceptualization, N.V.L. and T.K.A.; Data curation, S.O.C. and N.V.L.; Investigation, A.A.S., S.O.C. and T.A.S.; Methodology, N.V.L. and T.K.A.; Writing—original draft, N.V.L.; Writing—review and editing, T.K.A. and Y.N.M. All authors have read and agreed to the published version of the manuscript.

Funding: This work was financially supported by the Moscow Polytechnic University within the framework of the grant named after Pyotr Kapitsa (SEM, EMPA, XRD, HV) and by the Russian Science Foundation, grant number 22-79-00179 (electrochemical behavior).

Data Availability Statement: The raw/processed data required to reproduce these findings cannot be shared at this time due to technical or time limitations.

Acknowledgments: The authors would like to thank the JSC Aluminum Alloys Plant (JSC Aluminum Alloys Plant, 3K Metallurgov Ave., Podolsk, Moscow Oblast 142155, Russia) and, personally, the CEO Andrey G. Tsydenov for providing aluminum samples with PEO coating for the study.

Conflicts of Interest: The authors declare that they have no conflict of interest.

References

1. Polmear, I. *Light Alloys: From Traditional Alloys to Nanocrystals*, 4th ed.; Butterworth-Heinemann: Oxford, UK, 2006; pp. 216–226.
2. Belov, N.A.; Naumova, E.A.; Akopyan, T.K. *Aluminium-Based Eutectic Alloys: New Alloying Systems*; Ore and Metals PH: Moscow, Russia, 2016; pp. 191–235.

3. Akopyan, T.K.; Letyagin, N.V.; Avxentieva, N.N. High-tech alloys based on Al-Ca-La(-Mn) eutectic system for casting, metal forming and selective laser melting. *Non Ferr. Met.* **2020**, *1*, 52–59. [[CrossRef](#)]
4. Belov, N.A.; Naumova, E.A.; Akopyan, T.K.; Doroshenko, V.V. Phase Diagram of the Al-Ca-Fe-Si System and Its Application for the Design of Aluminum Matrix Composites. *JOM* **2018**, *70*, 2710–2715. [[CrossRef](#)]
5. Belov, N.A.; Naumova, E.A.; Doroshenko, V.V.; Korotkova, N.O.; Avxentieva, N.N. Determination of the Parameters of a Peritectic Reaction that Occurred in the Al-Rich Region of the Al-Ca-Mn System. *Phys. Met. Metallogr.* **2022**, *123*, 759–767. [[CrossRef](#)]
6. Letyagin, N.V.; Shurkin, P.K.; Nguen, Z.; Koshmin, A.N. Effect of Thermodeformation Treatment on the Structure and Mechanical Properties of the Al₃Ca1Cu_{1.5}Mn Alloy. *Phys. Met. Metallogr.* **2021**, *122*, 814–819. [[CrossRef](#)]
7. Akopyan, T.K.; Letyagin, N.V.; Sviridova, T.A.; Korotkova, N.O.; Prosviryakov, A.S. New Casting Alloys Based on the Al + Al₄(Ca,La) Eutectic. *JOM* **2020**, *72*, 3779–3786. [[CrossRef](#)]
8. Naumova, E.; Doroshenko, V.; Barykin, M.; Sviridova, T.; Lyasnikova, A.; Shurkin, P. Hypereutectic Al-Ca-Mn(-Ni) Alloys as Natural Eutectic Composites. *Metals* **2021**, *11*, 890. [[CrossRef](#)]
9. Shurkin, P.K.; Belov, N.A.; Musin, A.F.; Aksenov, A.A. Novel High-Strength Casting Al–Zn–Mg–Ca–Fe Aluminum Alloy without Heat Treatment. *Russ. J. Non-Ferr. Met.* **2020**, *61*, 179–187. [[CrossRef](#)]
10. Belov, N.A.; Akopyan, T.K.; Korotkova, N.O.; Naumova, E.A.; Pesin, A.M.; Letyagin, N.V. Structure and Properties of Al-Ca (Fe, Si, Zr, Sc) Wire Alloy Manufactured from As-Cast Billet. *JOM* **2020**, *72*, 3760–3768. [[CrossRef](#)]
11. Belov, N.A.; Naumova, E.A.; Ilyukhin, V.D.; Doroshenko, V.V. Structure and mechanical properties of Al–6% Ca–1% Fe alloy foundry goods, obtained by die casting. *Tsvetn. Met.* **2017**, *3*, 69–75. [[CrossRef](#)]
12. Fokin, D.; Matveev, S.; Vakhromov, R.; Alabin, A. Effect of Alloying Elements on Strength Properties and Casting Properties of Corrosion Resistant Quench-Free Al–Ca Alloys. In *Light Metals*; Eskin, D., Ed.; Springer: Cham, Switzerland, 2022; pp. 113–118.
13. Shurkin, P.K.; Letyagin, N.V.; Yakushkova, A.I.; Samoshina, M.E.; Ozherelkov, D.Y.; Akopyan, T.K. Remarkable thermal stability of the Al-Ca-Ni-Mn alloy manufactured by laser-powder bed fusion. *Mater. Lett.* **2021**, *285*, 129074. [[CrossRef](#)]
14. Rakoch, A.G.; Gladkova, A.A.; Dub, A.V. *Plasma Electrolytic Treatment of Aluminum and Titanium Alloys*; MISiS PH: Moscow, Russia, 2017; pp. 8–27.
15. Zhu, L.; Guo, Z.; Zhang, Y.; Li, Z.; Sui, M. A mechanism for the growth of a plasma electrolytic oxide coating on Al. *Electrochim. Acta* **2016**, *208*, 296–303. [[CrossRef](#)]
16. Li, Y.; Zhang, D.; Qi, C.; Xue, Y.; Wan, Y.; Sun, H. Enhanced corrosion and tribocorrosion behavior of plasma electrolytic oxidized coatings on 5052 aluminum alloy with addition of pullulan to silicate electrolyte. *J. Alloys Compd.* **2023**, *960*, 170782. [[CrossRef](#)]
17. Zhang, J.; Dai, W.; Wang, X.; Wang, Y.; Yue, H.; Li, Q.; Yang, X.; Guo, C.; Li, C. Micro-arc oxidation of Al alloys: Mechanism, microstructure, surface properties, and fatigue damage behavior. *J. Mater. Res. Technol.* **2023**, *23*, 4307–4333. [[CrossRef](#)]
18. Rodriguez, L.; Paris, J.-Y.; Denape, J.; Delbé, K. Micro-Arcs Oxidation Layer Formation on Aluminium and Coatings Tribological Properties—A Review. *Coatings* **2023**, *13*, 373. [[CrossRef](#)]
19. Wang, P.; Wu, T.; Xiao, Y.T.; Zhang, L.; Pu, J.; Cao, W.J.; Zhong, X.M. Characterization of micro-arc oxidation coatings on aluminum drill pipes at different current density. *Vacuum* **2017**, *142*, 21–28. [[CrossRef](#)]
20. Markov, M.A.; Bykova, A.D.; Krasikov, A.V.; Farmakovskii, B.V.; Gerashchenkov, D.A. Formation of Wear- and Corrosion-Resistant Coatings by the Microarc Oxidation of Aluminum. *Refract. Ind. Ceram.* **2018**, *59*, 207–214. [[CrossRef](#)]
21. Famiyeh, L.; Huang, X. Plasma Electrolytic Oxidation Coatings on Aluminum Alloys: Microstructures, Properties, and Applications. *Mod. Concept. Mater. Sci.* **2019**, *2*, 000526.
22. Gulec, A.E.; Gencer, Y.; Tarakci, M. The characterization of oxide based ceramic coating synthesized on Al-Si binary alloys by microarc oxidation. *Surf. Coat. Technol.* **2015**, *269*, 100–107. [[CrossRef](#)]
23. Li, K.; Li, W.; Zhang, G.; Zhu, W.; Zheng, F.; Zhang, D.; Wang, M. Effects of Si phase refinement on the plasma electrolytic oxidation of eutectic Al-Si alloy. *J. Alloys Compd.* **2019**, *790*, 650–656. [[CrossRef](#)]
24. Li, K.; Li, W.; Zhang, G.; Wang, M.; Tang, P. Influence of surface etching pretreatment on PEO process of eutectic Al-Si alloy. *Chin. J. Chem. Eng.* **2015**, *23*, 1572–1578. [[CrossRef](#)]
25. Cengiz, S.; Tarakci, M.; Gencer, Y.; Devecili, A.O.; Azakli, Y. Oxide based ceramic coating on Al-4Cu alloy by microarc oxidation. *Acta Phys. Pol. A* **2013**, *123*, 445–448. [[CrossRef](#)]
26. Agureev, L.; Savushkina, S.; Ashmarin, A.; Borisov, A.; Apelfeld, A.; Anikin, K.; Tkachenko, N.; Gerasimov, M.; Shcherbakov, A.; Ignatenko, V.; et al. Study of Plasma Electrolytic Oxidation Coatings on Aluminum Composites. *Metals* **2018**, *8*, 459. [[CrossRef](#)]
27. Tarakci, M. Plasma electrolytic oxidation coating of synthetic Al-Mg binary alloys. *Mater. Char.* **2011**, *62*, 1214–1221. [[CrossRef](#)]
28. Gencer, Y.; Tarakci, M.; Gulec, A.E.; Oter, Z.C. Plasma electrolytic oxidation of binary Al-Sn alloys. *Acta Phys. Pol. A* **2014**, *125*, 659–663. [[CrossRef](#)]
29. Gencer, Y.; Gulec, A.E. The effect of Zn on the microarc oxidation coating behavior of synthetic Al-Zn binary alloys. *J. Alloys Compd.* **2012**, *525*, 159–165. [[CrossRef](#)]
30. Cengiz, S. Synthesis of eutectic Al-18Ce alloy and effect of cerium on the PEO coating growth. *Mater. Chem. Phys.* **2020**, *247*, 122897. [[CrossRef](#)]
31. Oter, Z.C.; Gencer, Y.; Tarakci, M. The characterization of the coating formed by Microarc oxidation on binary Al-Mn alloys. *J. Alloys Compd.* **2015**, *650*, 185–192. [[CrossRef](#)]
32. Cosan, K.A.; Gunduz, K.O.; Tarakci, M.; Gencer, Y. Plasma electrolytic oxidation of as-cast and heat-treated binary Al-Ni alloys. *Surf. Coat. Technol.* **2022**, *450*, 128998. [[CrossRef](#)]

33. Rogov, A.B.; Lyu, H.; Matthews, A.; Yerokhin, A. AC plasma electrolytic oxidation of additively manufactured and cast AlSi12 alloys. *Surf. Coat. Technol.* **2020**, *399*, 126116. [[CrossRef](#)]
34. Liu, C.; Wang, Q.; Cao, X.; Cha, L.; Ye, R.; Ramachandran, C.S. Significance of plasma electrolytic oxidation treatment on corrosion and sliding wear performances of selective laser melted AlSi10Mg alloy. *Mater. Charact.* **2021**, *181*, 111479. [[CrossRef](#)]
35. Mora-Sanchez, H.; Olmo, R.; Rams, J.; Torres, B.; Mohedano, M.; Matykina, E.; Arrabal, R. Hard Anodizing and Plasma Electrolytic Oxidation of an Additively Manufactured Al-Si alloy. *Surf. Coat. Technol.* **2021**, *420*, 127339. [[CrossRef](#)]
36. Wu, T.; Blawerta, C.; Zheludkevich, M.L. Influence of secondary phases of AlSi9Cu3 alloy on the plasma electrolytic oxidation coating formation process. *J. Mater. Sci. Technol.* **2020**, *20*, 75–85. [[CrossRef](#)]
37. Polunin, A.V.; Cheretaeva, A.O.; Borgardt, E.D.; Rastegaev, I.A.; Krishtal, M.M.; Katsman, A.V.; Yasnikov, I.S. Improvement of oxide layers formed by plasma electrolytic oxidation on cast Al–Si alloy by incorporating TiC nanoparticles. *Surf. Coat. Technol.* **2021**, *423*, 127603. [[CrossRef](#)]
38. Shelekhov, E.V.; Sviridova, T.A. Programs for X-ray analysis of polycrystals. *Met. Sci. Heat Treat.* **2000**, *42*, 309–313. [[CrossRef](#)]
39. Pezzato, L.; Rigon, M.; Martucci, A.; Brunelli, K.; Dabala, M. Plasma Electrolytic Oxidation (PEO) as pre-treatment for sol-gel coating on aluminum and magnesium alloys. *Surf. Coat. Technol.* **2019**, *366*, 114–123. [[CrossRef](#)]
40. Fathi, P.; Mohammadi, M.; Duan, X.; Nasiri, A.M. A comparative study on corrosion and microstructure of direct metal laser sintered AlSi10Mg_200C and die cast A360.1 aluminum. *J. Mater. Process. Technol.* **2018**, *259*, 1–14. [[CrossRef](#)]
41. Yang, Y.; Chen, Y.; Zhang, J.; Gu, X.; Qin, P.; Dai, N.; Li, X.; Kruth, J.-P.; Zhang, L.-C. Improved corrosion behavior of ultrafine-grained eutectic Al-12Si alloy produced by selective laser melting. *Mater. Des.* **2018**, *146*, 239–248. [[CrossRef](#)]
42. Stevens, E.L.; Toman, J.; To, A.C.; Chmielus, M. Variation of hardness, microstructure, and Laves phase distribution in direct laser deposited alloy 718 cuboids. *Mater. Des.* **2017**, *119*, 188–198. [[CrossRef](#)]
43. Volkova, O.V.; Dub, A.V.; Rakoch, A.G.; Gladkova, A.A.; Samoshina, M.E. Comparison of pitting corrosion tendency for castings made of Al6Ca, Al1Fe, Al6Ca1Fe experimental alloys and AK12M2 industrial alloy. *Izv. Vuzov. Tsvetnaya Metall.* **2017**, *5*, 75–81. [[CrossRef](#)]
44. Kong, D.; Dong, C.; Ni, X.; Li, X. Corrosion of metallic materials fabricated by selective laser melting. *Mater Degrad.* **2019**, *3*, 24. [[CrossRef](#)]
45. Pezzato, L.; Dabalà, M.; Gross, S.; Brunelli, K. Effect of microstructure and porosity of AlSi10Mg alloy produced by selective laser melting on the corrosion properties of plasma electrolytic oxidation coatings. *Surf. Coat. Technol.* **2020**, *404*, 126477. [[CrossRef](#)]

Disclaimer/Publisher’s Note: The statements, opinions and data contained in all publications are solely those of the individual author(s) and contributor(s) and not of MDPI and/or the editor(s). MDPI and/or the editor(s) disclaim responsibility for any injury to people or property resulting from any ideas, methods, instructions or products referred to in the content.